HHS Public Access

Author manuscript

J Biomech. Author manuscript; available in PMC 2016 May 01.

Published in final edited form as:

J Biomech. 2015 May 1; 48(7): 1248–1257. doi:10.1016/j.jbiomech.2015.03.010.

Computational study of false vocal folds effects on unsteady airflows through static models of the human larynx

Charles Farbos de Luzan[a,*], **Jie Chen**[a], **Mihai Mihaescu**[b], **Sid M. Khosla**[c], and **Ephraim Gutmark**[a]

[a]Department of Aerospace Engineering and Engineering Mechanics, University of Cincinnati, Cincinnati, Ohio 45221-0070

[b]Department of Mechanics, Linné Flow Centre, School of Engineering Sciences, Royal Institute of Technology (KTH), Stockholm, Sweden

[c]Department of Otolaryngology-Head and Neck Surgery, University of Cincinnati Medical Center, Cincinnati, Ohio 45256-0528

Abstract

Compressible large eddy simulation is employed to numerically investigate the laryngeal flow. Symmetric static models of the human larynx with a divergent glottis are considered, with the presence of false vocal folds (FVFs). The compressible study agrees well with that of the incompressible study. Due to the high enough Reynolds number, the flow is unsteady and develops asymmetric states downstream of the glottis. The glottal jet curvature decreases with the presence of FVFs or the ventricular folds. The gap between the FVFs stretches the flow structure and reduces the jet curvature. The presence of FVFs has a significant effect on the laryngeal flow resistance. The intra-glottal vortex structures are formed on the divergent wall of the glottis, immediately downstream of the separation point. The vortices are then convected downstream and characterized by a significant negative static pressure. The FVFs are a main factor in the generation of stronger vortices, and thus on the closure of the TVFs. The direct link between the FVFs geometry and the motion of the TVFs, and by extension to the voice production, is of interest for medical applications as well as future research works. The presence of the FVFs also changes the dominant frequencies in the velocity and pressure spectra.

Keywords

LES; larynx; vocal folds

[*]Corresponding author: Tel: +1 513-556-1056. farboscs@mail.uc.edu (Charles Farbos de Luzan).

Conflict of interest

None of the authors have any financial and personal relationships with other people or organizations that could inappropriately influence (bias) their work.

1. Introduction

During human speech, the vocal folds are excited into self-sustained oscillations by the lung pressure that is applied to their inferior surfaces. The true vocal folds (TVFs) motion modulates the area between the vocal folds to an alternating convergent (during opening) and divergent (during closing) glottal duct. In computational models of normal phonation, it is usually assumed that the the larynx is symmetric relative to the anterior-posterior mid-plane and the TVFs vibrate in a symmetric fashion. However, the intra-glottal flow structure can be asymmetric despite of geometrical symmetry (Scherer et al., 2001, 2002; Shinwari et al., 2003; Mihaescu et al., 2007). At low flow rates, the glottal flow is laminar and can be attached or skewed to one of the folds due to the Coanda effect (Cherdron et al., 1978; Tsui and Wang, 1995). This phenomenon is typically observed for steady flow conditions (Pelorson et al., 1994; Hofmans et al., 2003; Scherer et al., 2001; Shinwari et al., 2003; Kucinschi et al., 2006). Also, asymmetric flows can naturally occur during phonation due to asymmetries in the vocal fold geometry.

The impact of the FVFs, or the ventricular folds, on the trans-glottal flow has also been studied (Scherer et al., 1983; Ikeda et al., 2001). The FVFs redirect skewed flow from the glottis and cause enhancement of low pressure in the glottis (Miller et al., 1988; Pelorson et al., 1994; Mihaescu et al., 2013). The FVFs also influence the vortical structures and pressure in the larynx. Miller et al. (1988) observed significant pressure recovery and jet reattachment with the presence of FVFs. An experimental study in a rigid laryngeal model suggested that FVFs straighten the glottal jet flow and reinforce its quasi-two-dimensionality (Chisari et al., 2011). The visualization results obtained in a 3:1 up-scaled dynamic glottis model in a water circuit showed that pressure loss is decreased when a second constriction is added downstream the glottis and the glottal jet is stabilized in the divergent phase of the cycle (Triep and Brücker, 2010). Bailly et al. (2008) concluded that asymmetrical seem quite limited under unsteady flow conditions created by a dynamical vocal fold replica. McGowan and Howe (2010) found that the rigid ventricle folds have negligible effect on the voice source when the vocal fold movement is specified by a simple mathematical model. The reason might be that the flow unsteadiness caused by the wall movement appears to be only significant in the case of the straight uniform vocal fold replica (Deverge et al., 2003). Numerical studies showed that the glottal jet can impinge on the FVFs, leading to a high-frequency dipole sound source (Zhang et al., 2002, e.g.). Using a rigid replica combining TVFs and FVFs, Agarwal (2004) linked the trans-laryngeal airflow resistance to the laryngeal geometry. However, Kucinschi et al. (2006) found that the pressure drop in the models with FVFs are very similar to those without FVFs at the same volumetric flow rate. Iijima et al. (1992) found that the effect of the FVFs was less significant for a convergent glottal shape than for a divergent or uniform shape.

With the development in computer technology and numerical methods, Computational Fluid Dynamics (CFD) has been used in a large range of applications. Unsteady CFD tools have investigated two-dimensional, axisymmetric, and three-dimensional glottal configurations with and without vocal fold motion (Zhao et al., 2002; Zhang et al., 2002; Hofmans et al., 2003; Alipour and Scherer, 2004; Suh and Frankel, 2007; Mihaescu et al., 2010). Only a few studies have been discussed on the effects of the FVFs. Farahani et al. (2013) investigated

the incompressible laryngeal flow for a geometry including FVFs, but did not account for the divergent phase in the cycle of the TVFs. Also, other studies have considered the reconstruction of subject-specific geometries using computed tomography data such as the work by (Bakhshaee et al., 2013). Xue et al. (2014) analyzed the phonation cycle using flow structure interaction (FSI) and an incompressible solver for the Navier-Stokes equations. Nevertheless, most of the research to date has tended to focus on parametric models, which remains a way to isolate and understand better the contribution from specific parts of the larynx to the human phonation.

The present study numerically explores the unsteady trans-glottal flow structure during the divergent phase of the TVFs motion. In order to investigate the FVFs effects, static laryngeal models with and without the presence of the FVFs just downstream the TVFs are considered. Time-averaged velocity and pressure, as well as their fluctuations, are utilized in the discussion. Spectral analyses of frequency are performed to find the flows dominant frequency mode. The FVFs effects on the flow resistance and on the developed instabilities are also discussed.

2. Methods

Unsteady large eddy simulation (LES) (Fluent Inc.®) is employed to investigate the incompressible and the compressible laryngeal airflows. This solver has been validated in previous studies (Mylavarapu et al., 2009; Mihaescu et al., 2011). Nine three-dimensional static and diverging larynx models with and without FVFs are considered. Fig. 1 shows the schematic of the two-dimensional cross-section of the baseline (without FVFs) (a) and of the symmetric larynx model with FVFs (b) as well as its main dimensions. A three-dimensional view of the baseline model is also shown (c). The length of the sub-glottal region is 10 mm. The TVFs shape is characterized by a 20° divergent angle corresponding to the closing phase of the phonation cycle. The *x*-*y* plane represents the axial plane, the *x*-*z* plane represents the sagittal plane and the *y*-*z* plane represents the coronal plane. The computational domain consists of a square cross-section of 15.24 mm × 15.24 mm in the axial plane, and 60 mm in the stream-wise direction (*z*). The length of the glottis is the same as that of the false folds and of the computational cross-section, 15.24 mm. The glottal width (D_g), which is the minimum distance between the TVFs, is 1.6 mm. The FVFs shape is characterized by a 40° divergent angle. Two ventricle sizes (h_v) are considered to investigate the influence of the cavity resonance on the flow structures, so the FVFs are placed downstream from the glottal exit at 6 mm and 2.67 mm. The geometry and sizes are similar to Kucinschi et al. (2006). Four sets of flow gap between the FVFs (D_{FVF}) are considered in this study: 3 mm, 4.5 mm, 6.23 mm and 8.58 mm, respectively. These values fall in the range studied by Agarwal (2004). The length of the supra-glottal region varies from case to case because the total stream-wise length of the computational domain is kept constant at 60 mm. The computational domain is discretized into approximately 1.5×10^6 unstructured hexahedral mesh volumes.

Second order finite volume schemes are employed to discretize the flow governing equations on the computational domain. The time integration is performed using an implicit second order discretization scheme. The semi-implicit method for pressure-linked equation

(SIMPLE) algorithm is applied to solve the coupling between the pressure field and velocity field (Patankar and Spalding, 1972). The wall-adapting local eddy-viscosity (WALE) model is employed as the subgrid-scale model in this study (Nicoud and Ducros, 1999). The simulations are conducted under uniform inlet and outlet pressure boundary conditions. To follow the study performed by Mihaescu et al. (2013), the trans-glottal pressure is 687 Pa (7 cm H_2O), which corresponds to a normal conversation level. The Reynolds number based on the glottal width is around 3600 at the narrowest location of the glottis. The compressible flow solver is employed for a complete characterization of the flow field in the tract. No-slip boundary conditions for velocity are set at the solid boundaries of the computational domain. A converged solution based on a steady state RANS solution with standard k-ε turbulence model is used to initialize the LES simulations. The time step used in the study is $\Delta t = 2.0 \times 10^{-5}$s. The mean flow quantities are statistically averaged over a period of 10,000 time-steps. Based on the time step and the total running time, the frequencies can be computed in the range of 5–50,000 Hz.

3. Results

The general behavior of the flow in the baseline glottal configuration, without FVFs, is investigated. Then, the flow through different glottal configurations that include the FVFs is explored to establish a connection between the flow structures.

3.1. Baseline Case: no FVFs

This study sets out to be a foundation to a broader range of investigations such as the acoustic effects of FVFs on the human phonation. The compressible flow solution includes acoustic information, since the unsteady compressible Navier-Stokes equations describe both the vortical field and the aerodynamically generated sound. Thus a compressible solver is preferred over an incompressible one. It is assumed that the Reynolds number is low enough to assume that incompressible and compressible solvers will show similar results, due to the low flow rates that occur in the human larynx. The baseline case (without FVFs) is computed for the two solvers and velocity components are extracted along the line going through the TVFs where the Reynolds number is the largest. As one can see on fig. 2 the comparison of the two cases allows considering that in the region nearby the throat, the compressible solution is very similar to the incompressible flow. From now on, only the compressible solution will be discussed.

The characteristic frequencies in the flow field are examined using velocity and pressure spectra. The spectra are obtained by recording the axial velocity and static pressure time-history at monitoring points and performing discrete Fourier transforms on these data sets. Fig. 3 (a) shows two monitoring points in the baseline case, point $M1$ is located in the glottal area while $M2$ is positioned downstream of the glottal exit. Monitoring point $M2$ is chosen to be outside of the glottal flow, in order to capture radiating pressure waves from the jet. Fig. 3 (b) shows the velocity spectrum at point $M1$ while Fig. 3 (c) shows the pressure spectrum at point $M2$. The dominant frequencies at these two points, and in many additional points are found to be at 2525 Hz. Based on the minimum glottal width (D_g) and the mean velocity of the glottal jet at this location ($W \sim 32.8$ m/s), the Strouhal number ($St = fD_g/W$) is 0.12. It was found that high frequency induced by vortex shedding in the supra-glottal

region is related to shear layer instability (Mihaescu et al., 2010). Experimental studies found the Strouhal number of vortex shedding is approximately 0.145 for glottal flows with the Reynolds number roughly 2000 (Kucinschi et al., 2006; Zhang et al., 2004). This is slightly higher than that in our finding.

3.2. False Vocal Folds Effects

The time-averaged axial velocity distributions in the mid-coronal plane (*y*-*z* mid-plane) of all eight cases with FVFs are shown in Fig. 4. The ventricle length, h_v represents the distance between the TVFs and the FVFs. As seen in Fig. 4 (a) (h_v = 2.67 mm), the flow is shifted towards the top wall. While in Fig. 4 (b) (h_v = 2.67 mm), the flow is skewed towards the other side. In order to simplify the discussion in the following sections, the side which the flow attaches to is called ‘flow side’ while the side which the flow separates from is called ‘no-flow side’. The glottal jet skews less as the gap, D_{FVF} is decreasing. This trend is slightly more accentuated as h_v is increased. In the cases that the glottal jet is completely straightened downstream of the TVFs, it still deflects downstream of the FVFs. With the same pressure drop applied from the inlet to the outlet of the computational domains, the narrower the D_{FVF} is, the larger the maximum velocity in the glottis is.

The time-averaged and rms axial velocity profiles through the TVFs and the FVFs are presented in Figs. 5 and 6. The six places chosen are at the location of minimum glottal area between TVFs, the exit of TVFs, halfway between TVFs and FVFs, the throat, halfway, and exit of the FVFs. As noticed in Fig. 4, the jet is bistable, skewing randomly to either side of the folds. In order to compare the jet velocity mean and rms profiles, the jets that were tilted towards the upper wall were mirrored relative to the centerline such that they match the tilt downwards. The narrower the D_{FVF} is, the closer the jet is to the centerline. D_{FVF} also plays an important role on the rms axial velocity. As the FVFs gap decreases, the rms on the detached side of the jet increases. This trend is clearer with the smaller ventricle.

The normalized flow resistance with respect to the baseline case is presented in Fig. 7. The gap between the FVFs, D_{FVF}, is normalized by the gap between the TVFs (D_g = 1.6 mm). The flow resistance is defined as the pressure drop divided by the mean volumetric flow rate (Agarwal, 2004). For instance, the time-averaged pressures at locations A and B on the mid-coronal plane to the flow side are obtained as $p_{\mathrm{A,flowside}}$ and $p_{\mathrm{B,flowside}}$, then the flow resistance R is defined as

$$R=\frac{p_{\mathrm{A,flowside}}-p_{\mathrm{B,flowside}}}{Q} \quad (1)$$

where Q is the time-averaged volumetric flow rate. The resulting resistance R is normalized by the resistance at baseline, i.e. without considering the FVFs. The flow resistance of the no-flow side is defined the same way. The flow resistance with the narrowest considered D_{FVF} is lower than the resistance at Baseline (without FVFs) and it increases with increasing D_{FVF}, approaching for the largest D_{FVF} the resistance of the tract of without FVFs for the largest D_{FVF}. It is expected that as the distance between the FVFs is increased, their impact on R will decrease and approach the no-FVFs case. The theoretical work by Bailly et al. (2008) predicted that the normalized flow resistance can become smaller than

unity for a small region of D_{FVF}, when a pressure of 500 Pa is applied on a static vocal fold replica as the trans-glottal pressure. The trend of the resistance change with D_{FVF} is opposite to the present results and to Agarwal (2004). The geometry in the study by Bailly et al. (2008) is quite different from the present one and from that of Agarwal (2004). The lowest normalized resistance for the vocal tract is captured for $D_{FVF}/Dg = 2.8$, while in the present study and that of (Agarwal, 2004) around $D_{FVF}/Dg = 2$. Agarwal (2004) results shown in Fig. 7 are from the measurement on a static model with $D_g = 1.6$ mm and a 20° divergent glottis, which are the same as the values investigated in the present study. The range of the trans-glottal pressure, from 1 to 25 cm H_2O, was found to have negligible effects on the normalized flow resistance. In the present study a trans-glottal pressure of, 7 cm H_2O is employed.

The velocity and pressure spectra in Fig. 3 show the characteristic frequencies of the glottal flow in the cases with the presence of FVFs for the case with $D_{FVF} = 8.58$ mm and $h_v = 2.67$ mm. The spectra are obtained in the same manner as discussed for in the baseline case. Fig. 3 (d) shows two of the monitoring points locations, while Fig. 3 (e) exhibits the velocity spectrum at point *M*1 and Fig. 3 (f) presents the pressure spectrum at point *M*4. Many other monitoring points are also investigated, and the dominant frequencies are all the same, around 2650 Hz. This is higher than that in the baseline case, which was 2525 Hz. Based on the minimum glottal width and the mean velocity at the minimum cross-sectional glottal area ($W \sim 34.8$ m/s), the Strouhal number is estimated to be approximately 0.13.

Fig. 8 (a) shows the dominant frequencies observed for all the configurations analyzed in the present study. The solid line represents the frequency at Baseline of 2525 Hz, without the presence of FVFs. The dominant frequencies in the cases with FVFs are higher than in the baseline case. As D_{FVF} increases, the frequencies drop almost linearly approaching the value of no FVFs. The size of the ventricle has effect only at the two smallest gaps. The larger ventricle results in slightly lower frequencies than the smaller one. Figure 8 (b) shows the Strouhal numbers for the cases presented in Fig. 8 (a). The Strouhal number is based on the minimum glottal width (D_g), which is the gap between the TVFs, and the mean velocity at the minimum cross-sectional glottal area (W). The solid line shows the Strouhal number of the baseline case, approximately 0.12. The Strouhal numbers for the cases with FVFs are slightly higher than the baseline case with no clear trend. The larger ventricle has lower Strouhal number compared to the smaller one, approaching the no-FVFs case value. The Strouhal numbers are in good agreement with the experimental study (Kucinschi et al., 2006). It further indicates that high frequency in the supra-glottal region is related to shear layer instability (Mihaescu et al., 2010).

The streamlines of projected velocity vectors on a magnified view of the diverging part of the TVFs in the mid-plane are shown on Fig. 9. For each case, the detachment of the main stream that was observed on Fig. 4, generates vortical structures along the straight part of the walls in the diverging area. The current paper intends to prove the influence of the FVFs on the intensity of these vortices, and consequently on the collapsing force that is applied on the TVFs. Stevens (2000) discussed this force as being a contributor to the asymmetric collapse of the TVFs, and highlighted the importance of the closing phase of the cycle of sound production. Nomura et al. (2010) studied the effect of physical asymmetries on mechanical

models and identified them as a key factor in the harmonics produced in the voice. To prove the contribution of the FVFs to this force, a quantitative analysis of the vortical intensity was performed following the work of Cuppoletti (2013). Indeed, in the plane of study *yz*, the normal component of vorticity (ω_x) can be related to the circulation (Γ_x) of the flow in the diverging region of the TVFs. Γ_x was so calculated as in Eq. (2), on a window defined as the restriction of the mid-plane to the *z* coordinates comprised between *z* = 16.31 mm and *z* = 19.30 mm, which corresponds to the bounding planes of the straight portions of the diverging region of the TVFs.

$$\Gamma_x = \iint |\omega_x| \, dy \, dz \quad (2)$$

where $|\omega_x|$ is the absolute value of the normal vorticity with respect to the *yz*-plane. The results of this integration are shown on Fig. 10 (a). They are normalized by the value of Γ_x computed in the same location for the baseline case (without FVFs), which is represented by the dashed line. The diamonds represent the cases with the smaller ventricle size (h_v = 2.67 mm), the squares represent the other cases (h_v = 6 mm). D_{FVF} is normalized by the gap between the TVFs (D_g = 1.6 mm). Strong evidence of the influence of the gap size between the FVFs (D_{FVF}) is shown and it appears that the smaller the gap is, the more important the circulation is in the divergent part of the TVFs. More importantly, it is noticeable that the distance between the TVFs and the FVFs has an impact on the circulation as well, but not as much as D_{FVF}, which remains the main trigger of these vortices. In order to quantify the force applied to the walls, the static pressure is integrated over the diverging walls of the TVFs. Fig. 10 (b) shows the forces applied to the walls of the diverging section of the TVFs. Forces are normalized by the maximum value of the force computed for the baseline case (no FVFs). As in Fig. 10 (a), D_{FVF} is normalized by D_g. The squares represent the cases where h_v = 6 mm and the diamonds represent the case where h_v = 2.67 mm. A positive value of the force helps the TVFs to collapse. Regarding the trends, it appears that the collapsing forces get higher when D_{FVF} reduces. The ventricle size also has an impact on this effect since the strength of the forces is slightly lower in the case of the smaller h_v. Moreover, a correlation is found between the circulation and the calculated forces, where the trends overlap perfectly. It is important to notice the asymmetry in the forces applied to the walls for each case, which induces an asymmetric motion of the collapsing TVFs. When the gap between the FVFs reduces in size, this circulation phenomenon induces an asymmetric motion of the TVFs that generates a richer range of harmonics in the voice mechanism.

4. Discussions and conclusion

The impact of the FVFs on the flow field and acoustics of a static model of the human larynx was studied using compressible LES. Because of the low Mach number ($M < 0.3$) of the flow, the solutions of the incompressible and compressible LES were very similar in most locations.

The convergent geometry of the sub-glottis causes the flow to accelerate into the glottis. The flow decelerates downstream of the narrowest point due to the sudden expansion of the geometry in the axial direction during closing. The resulting adverse pressure gradient

separates the flow from the divergent sides of the glottis. The jet exiting the glottis is bistable; it can alternately skew toward one side or the other due to random downstream disturbances. However, asymmetric flow might occur during phonation due to asymmetries in the vocal fold geometry. It is still unclear whether or not the phenomenon that the flow attaches to one wall plays a role in the phonation.

The gap between the FVFs impacts more on the laryngeal airflow patterns than the the ventricle size h_v. The glottal jet curvature due to jet skewing is highest for the case without FVFs and decreases with the presence of FVFs such that the jet is virtually straight with the narrowest gap between the FVFs. This effect is more pronounced with an increased ventricle size. With the same pressure drop applied on the computational domain, the narrower the gap between FVFs is, the larger the maximum velocity in the glottis will be, which is a result of a flow resistance reduction when D_{FVF} decreases. The flow resistance is also more reduced with an increased ventricle size. When the FVFs gap increases, the resistance converges towards the one calculated without FVFs.

Experimental studies indicated that the Strouhal number of vortex shedding is approximately 0.145 for glottal flows with Reynolds number of roughly 2000 (Kucinschi et al., 2006; Zhang et al., 2004). In current study, with Re = 3200, the spectral analysis reveals that the velocity and pressure spectra have the same dominant frequencies for the same geometry. Without considering the FVFs, the vortices developed in the supra-glottal region are characterized by high frequencies around f = 2525 Hz, (St~ 0.12). Considering the FVFs effect, it increases this dominant frequency for all the investigated FVFs gaps (St~ 0.13–0.135). However, considering the FVFs effect, it was observed that the dominant frequencies are decreasing when increasing D_{FVF}. Dominant frequencies presented by Mihaescu et al. (2010) were based on velocity data in the glottal jet shear-layers from incompressible LES calculations. The Strouhal numbers given by Mihaescu et al. (2010) agree with the present results.

Finally, the key contributions of the current study are the following: (a) the study of the vortices that are generated in the divergent TVFs has shown that the geometry of the larynx, and more specifically of the FVFs gap, has an important impact on the human phonation mechanism; (b) a direct correlation between D_{FVF} and the strength of these recirculations was established, and the asymmetric effect it has on the collapsing of the TVFs was investigated. These points add to the fundamental knowledge on the role of the FVFs and may help to enhance clinician assessments and future medical research on the topic of voice production, by according a more important importance to the role of the FVFs.

The major limitations of this study were the following: (a) the use of a static model for the human larynx only allows to study one particular configuration of the motion cycle of the TVFs. Future work may aim at reconstructing a complete cycle by adding to this set of simulations several other static models corresponding to the main key configurations. An unsteady FSI study could also be considered in order to achieve this goal; (b) As stated before, this study uses parametric models, which do not account for the complex shapes of subject-specific larynges. Future studies may address this point by attempting to validate the

current models with subject-specific geometries reconstructed by computed tomography scans that match the current configuration (similar $D_{FV\,F}$, similar h_v, divergent TVFs).

In summary, the present study employed LES approach to investigate the effects of the FVFs on the airflow through human larynx models. The results suggest that the FVFs modify the flow field and affect the dominant unsteady velocity frequencies and the resulting pressure fluctuations.

Acknowledgments

This project was supported by NIH Grant No. R01 DC009435 from the National Institute of Deafness and Other Communication Disorders. This work was supported in part by an allocation of computing time from the Ohio Supercomputer Center.

References

Agarwal, M. PhD thesis. Bowling Green State University; 2004. The false vocal folds and their effect on translaryngeal airflow resistance.

Alipour F, Scherer RC. Flow separation in a computational oscillating vocal fold model. Journal of the Acoustical society of America. 2004; 116(3):1710–1719. [PubMed: 15478438]

Bailly L, Pelorson X, Henrich N, Ruty N. Influence of a constriction in the near field of the vocal folds: Physical modeling and experimental validation. The Journal of the Acoustical Society of America. 2008; 124(5):3296–3308. [PubMed: 19045812]

Bakhshaee H, Moro C, Kost K, Mongeau L. Three-dimensional reconstruction of human vocal folds and standard laryngeal cartilages using computed tomography scan data. Journal of Voice. 2013; 27(6):769–777. [PubMed: 24119643]

Cherdron W, Durst F, Whitelaw JH. Asymmetric flows and instabilities in symmetric ducts with sudden expansions. Journal of Fluid Mechanics. 1978; 84(01):13–31.

Chisari N, Artana G, Sciamarella D. Vortex dipolar structures in a rigid model of the larynx at flow onset. Experiments in Fluids. 2011; 50(2):397–406.

Cuppoletti, DR. PhD thesis. University of Cincinnati; 2013. Supersonic jet noise reduction with novel fluidic injection techniques.

Deverge M, Pelorson X, Vilain C, Lagrée PY, Chentouf F, Willems J, Hirschberg A. Influence of collision on the flow through in-vitro rigid models of the vocal folds. The Journal of the Acoustical Society of America. 2003; 114(6):3354–3362. [PubMed: 14714815]

Farahani MH, Mousel J, Alipour F, Vigmostad S. A numerical and experimental investigation of the effect of false vocal fold geometry on glottal flow. Journal of biomechanical engineering. 2013; 135(12):121006. [PubMed: 24008864]

Hofmans G, Groot G, Ranucci M, Graziani G, Hirschberg A. Unsteady flow through in-vitro models of the glottis. The Journal of the Acoustical Society of America. 2003; 113(3):1658–1675. [PubMed: 12656399]

Iijima H, Niki N, Nagai N. Glottal impedance based on a finite element analysis of two-dimensional unsteady viscous flow in a static glottis. Signal Processing, IEEE Transactions on. 1992; 40(9): 2125–2135.

Ikeda T, Matsuzaki Y, Aomatsu T. A numerical analysis of phonation using a two-dimensional flexible channel model of the vocal folds. Journal of biomechanical engineering. 2001; 123(6): 571–579. [PubMed: 11783728]

Kucinschi BR, Scherer RC, DeWitt KJ, Ng TT. Flow visualization and acoustic consequences of the air moving through a static model of the human larynx. Journal of biomechanical engineering. 2006; 128(3):380–390. [PubMed: 16706587]

McGowan RS, Howe MS. Influence of the ventricular folds on a voice source with specified vocal fold motion. The Journal of the Acoustical Society of America. 2010; 127(3):1519–1527. [PubMed: 20329852]

Mihaescu M, Gutmark E, Khosla S, Scherer R, Fuchs L. Flow and acoustics simulations based on les and an acoustic analogy; an application to laryngeal airflow. AIAA Paper No AIAA 919. 2007

Mihaescu, M.; Khosla, SM.; Ephraim, GJ. Quantification of the false vocal-folds effects on the intra-glottal pressures using large eddy simulation. Proceedings of Meetings on Acoustics; Acoustical Society of America; 2013. p. 060302

Mihaescu M, Khosla SM, Murugappan S, Gutmark EJ. Unsteady laryngeal airflow simulations of the intra-glottal vortical structures. The Journal of the Acoustical Society of America. 2010; 127(1): 435–444. [PubMed: 20058989]

Mihaescu M, Mylavarapu G, Gutmark EJ, Powell NB. Large eddy simulation of the pharyngeal airflow associated with obstructive sleep apnea syndrome at pre and post-surgical treatment. Journal of biomechanics. 2011; 44(12):2221–2228. [PubMed: 21700289]

Miller J, Pereira J, Thomas D. Fluid flow through the larynx channel. Journal of sound and vibration. 1988; 121(2):277–290.

Mylavarapu G, Murugappan S, Mihaescu M, Kalra M, Khosla S, Gutmark E. Validation of computational fluid dynamics methodology used for human upper airway flow simulations. Journal of biomechanics. 2009; 42(10):1553–1559. [PubMed: 19501360]

Nicoud F, Ducros F. Subgrid-scale stress modelling based on the square of the velocity gradient tensor. Flow, Turbulence and Combustion. 1999; 62(3):183–200.

Nomura H, Kamakura T, Funada T. Effects of vocal fold asymmetry on pressure wave fluctuations in a mechanical model. Acoustical Science and Technology. 2010; 31(2):148–155.

Patankar SV, Spalding DB. A calculation procedure for heat, mass and momentum transfer in three-dimensional parabolic flows. International Journal of Heat and Mass Transfer. 1972; 15(10):1787–1806.

Pelorson X, Hirschberg A, Van Hassel R, Wijnands A, Auregan Y. Theoretical and experimental study of quasisteady-flow separation within the glottis during phonation. application to a modified two-mass model. The Journal of the Acoustical Society of America. 1994; 96(6):3416–3431.

Scherer RC, Shinwari D, De Witt KJ, Zhang C, Kucinschi BR, Afjeh AA. Intraglottal pressure profiles for a symmetric and oblique glottis with a divergence angle of 10 degrees. The Journal of the Acoustical Society of America. 2001; 109(4):1616–1630. [PubMed: 11325132]

Scherer RC, Shinwari D, De Witt KJ, Zhang C, Kucinschi BR, Afjeh AA. Intraglottal pressure distributions for a symmetric and oblique glottis with a uniform duct (l). The Journal of the Acoustical Society of America. 2002; 112(4):1253–1256. [PubMed: 12398430]

Scherer RC, Titze IR, Curtis JF. Pressure-flow relationships in two models of the larynx having rectangular glottal shapes. The Journal of the Acoustical Society of America. 1983; 73(2):668–676. [PubMed: 6841807]

Shinwari D, Scherer RC, DeWitt KJ, Afjeh AA. Flow visualization and pressure distributions in a model of the glottis with a symmetric and oblique divergent angle of 10 degrees. The Journal of the Acoustical Society of America. 2003; 113(1):487–497. [PubMed: 12558286]

Stevens, KN. Acoustic phonetics. Vol. 30. MIT press; 2000.

Suh J, Frankel SH. Numerical simulation of turbulence transition and sound radiation for flow through a rigid glottal model. The Journal of the Acoustical Society of America. 2007; 121(6):3728–3739. [PubMed: 17552723]

Triep M, Brücker C. Three-dimensional nature of the glottal jet. The Journal of the Acoustical Society of America. 2010; 127(3):1537–1547. [PubMed: 20329854]

Tsui YY, Wang CK. Calculation of laminar separated flow in symmetric two-dimensional diffusers. Journal of fluids engineering. 1995; 117(4):612–616.

Xue Q, Zheng X, Mittal R, Bielamowicz S. Subject-specific computational modeling of human phonation. The Journal of the Acoustical Society of America. 2014; 135(3):1445–1456. [PubMed: 24606281]

Zhang C, Zhao W, Frankel SH, Mongeau L. Computational aeroacoustics of phonation, part ii: Effects of flow parameters and ventricular folds. The Journal of the Acoustical Society of America. 2002; 112(5):2147–2154. [PubMed: 12430826]

Zhang Z, Mongeau L, Frankel SH, Thomson S, Park JB. Sound generation by steady flow through glottis-shaped orifices. The Journal of the Acoustical Society of America. 2004; 116(3):1720–1728. [PubMed: 15478439]

Zhao W, Zhang C, Frankel SH, Mongeau L. Computational aeroacoustics of phonation, part i: Computational methods and sound generation mechanisms. The Journal of the Acoustical Society of America. 2002; 112(5):2134–2146. [PubMed: 12430825]

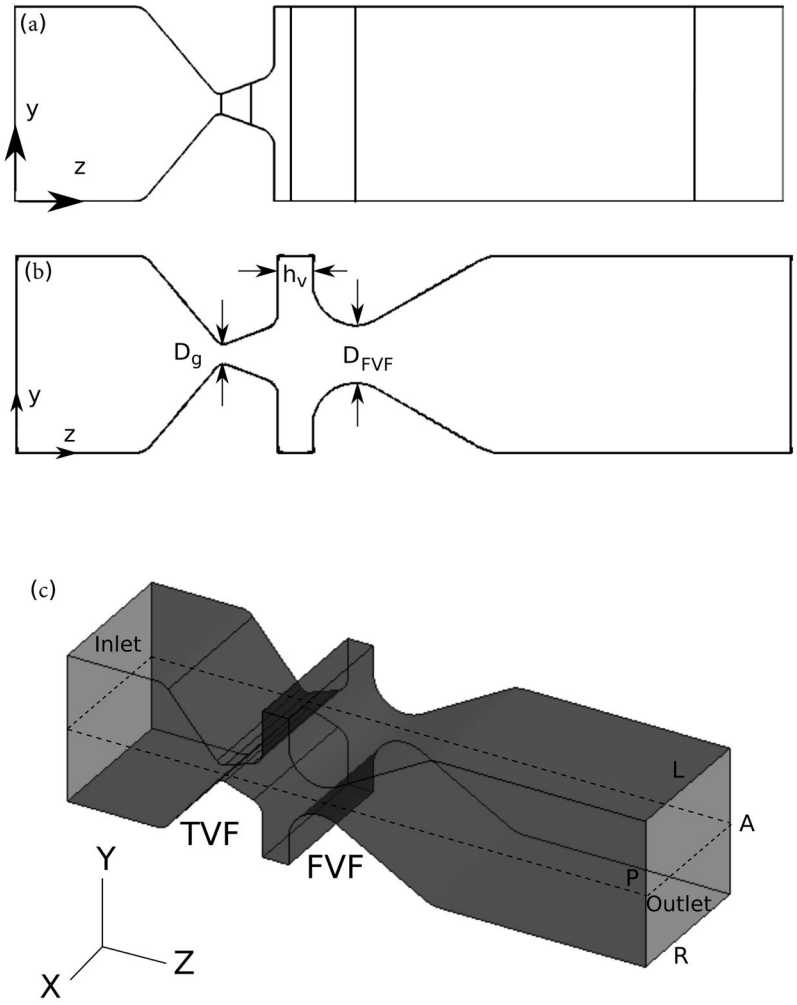

Figure 1.

Schematic of the cross-section of the larynx models. (a) baseline geometry. (b) model including FVFs. D_g: glottis width; h_v: ventricular height; D_{FVF} : gap between FVFs. (c) three-dimensional larynx model

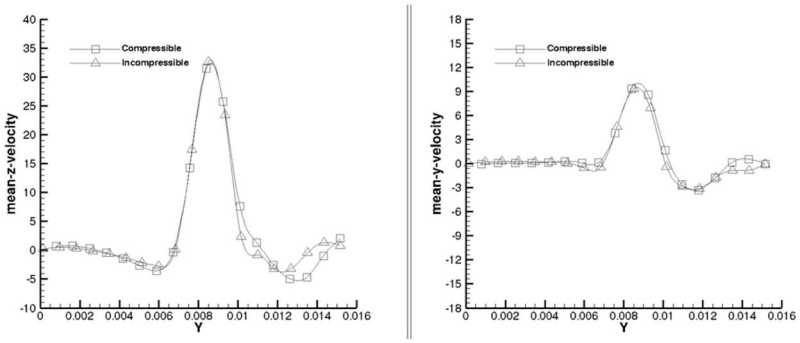

Figure 2.

Time-averaged axial velocity profiles in the mid-coronal plane at different axial locations (*z*). Solid lines - incompressible solution, circles - compressible solution.

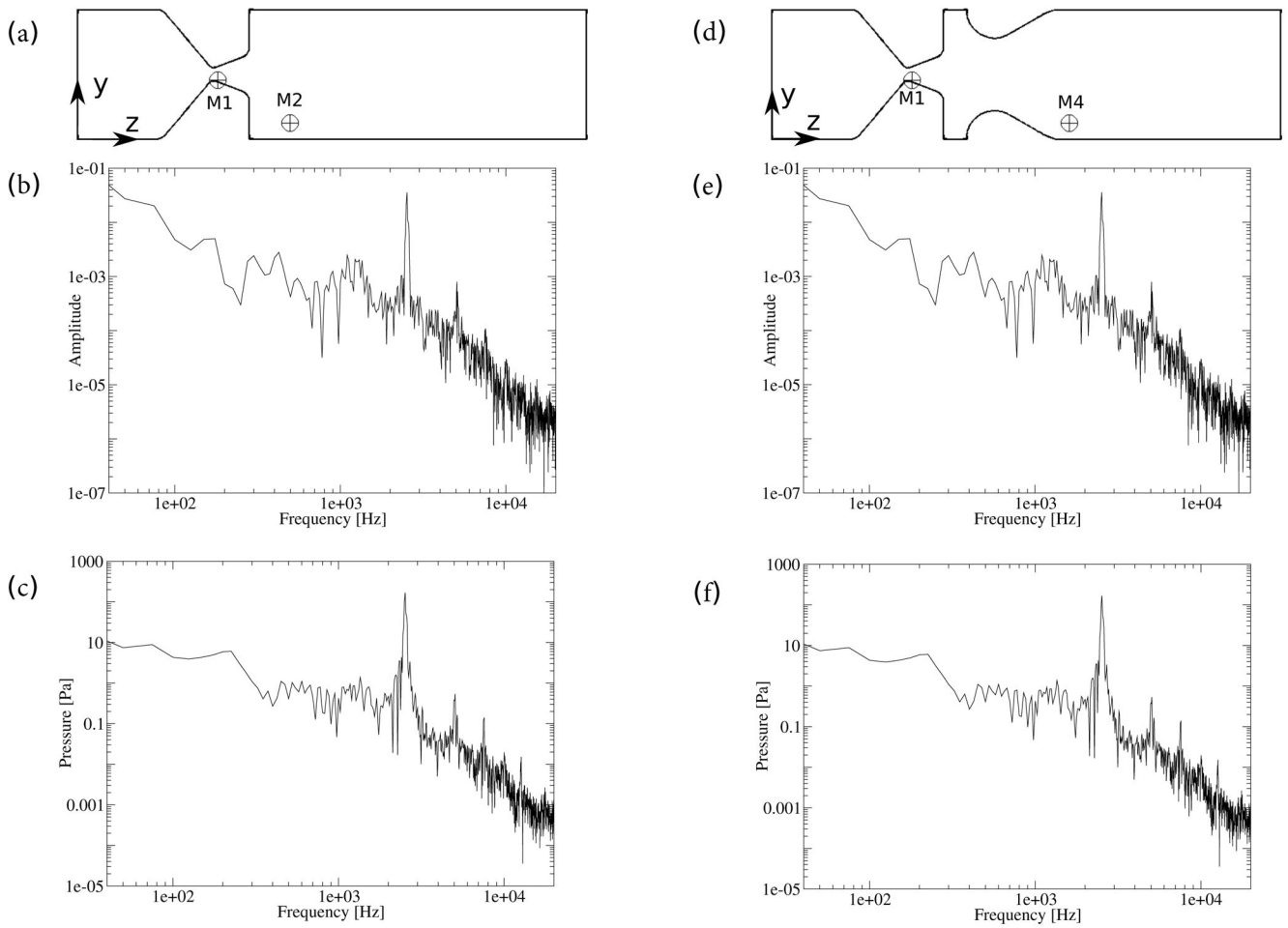

Figure 3.

(left) Frequency spectra of the vortical structures in the baseline case: (a) the locations of the monitoring points (*M*1 and *M*2); (b) velocity spectrum at *M*1; (c) pressure spectrum at *M*2. (right) Frequency spectra of the glottal flow in the case of D_{FVF} = 8.58 mm and h_v = 2.67 mm: (d) the location of the monitoring points (*M*1 and *M*4); (e) velocity spectrum at *M*1; (f) pressure spectrum at *M*4.

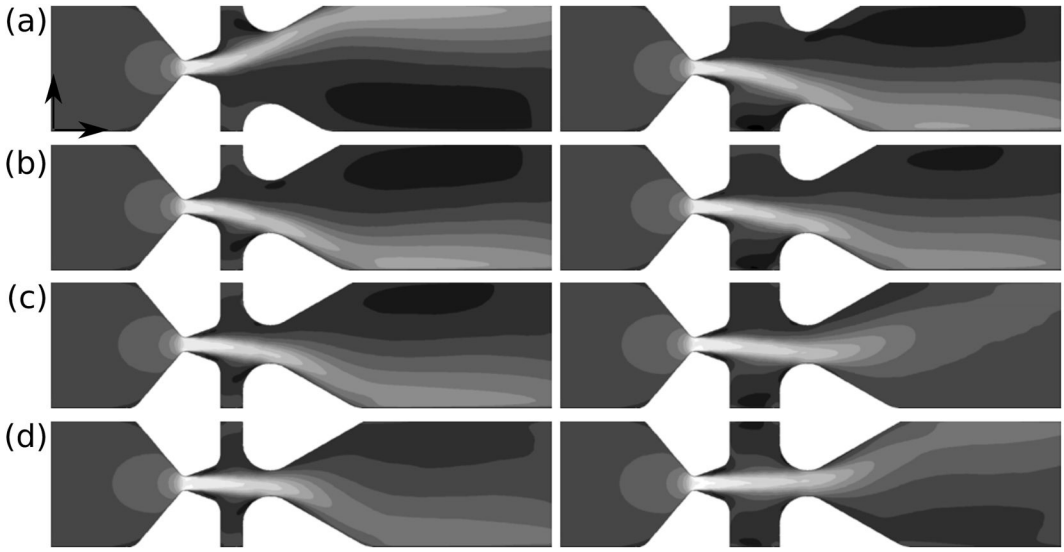

Figure 4.

Time-averaged axial velocity distribution in the mid-coronal plane at different D_{FVF} : (a) 8.58 mm, (b) 6.23 mm, (c) 4.5 mm, and (d) 3 mm. The left ones are the cases of h_v = 2.67 mm and the right ones are the cases of h_v = 6 mm.

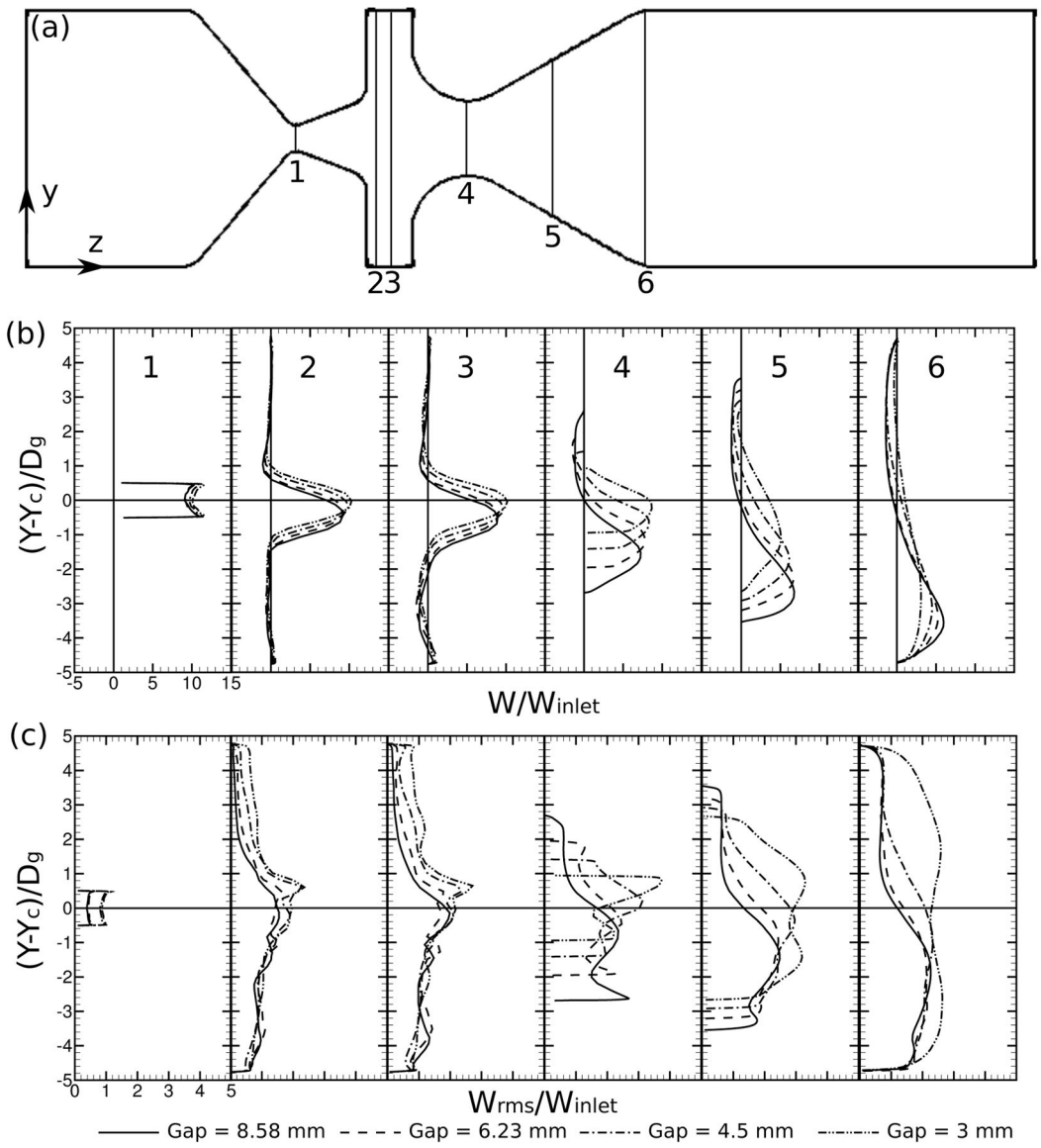

Figure 5.
Time-averaged and rms axial velocity profiles of h_v = 2.67 mm.

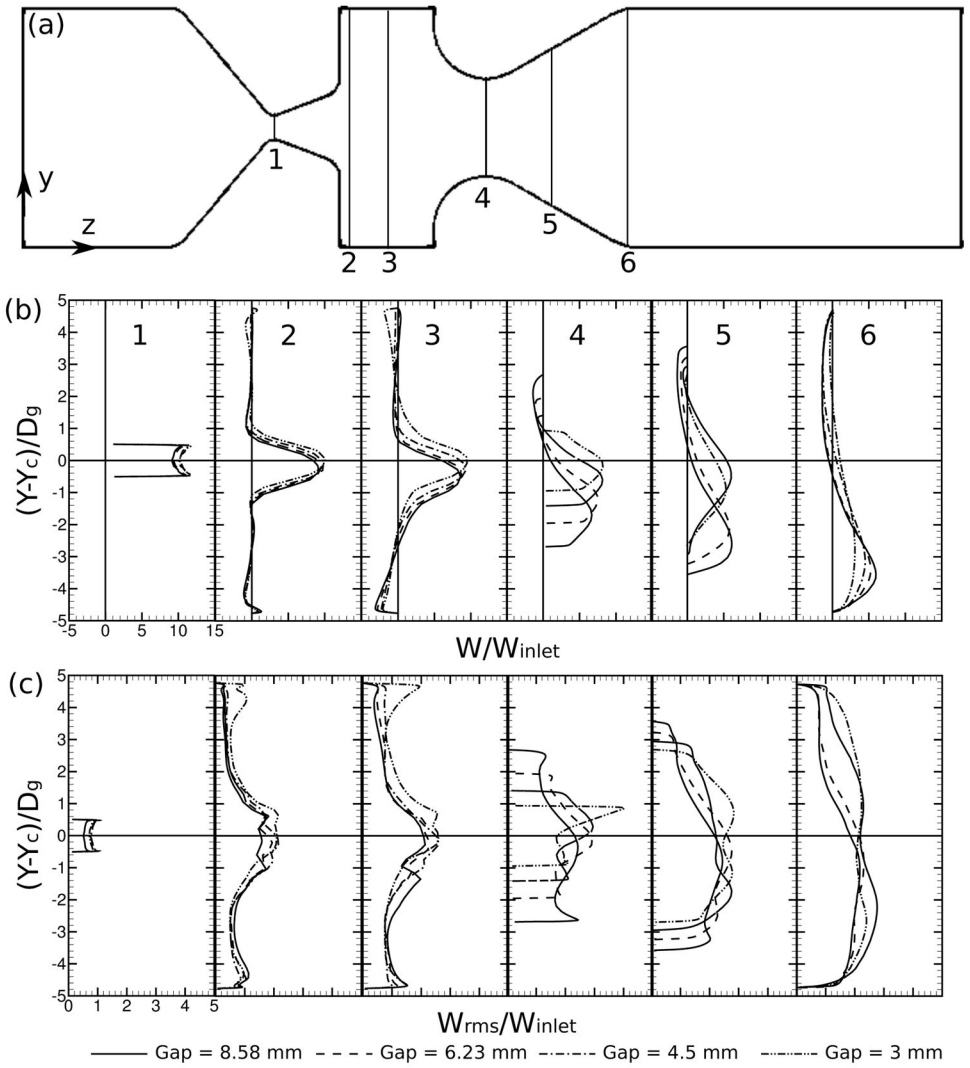

Figure 6.
Time-averaged and rms axial velocity profiles of h_v = 6 mm.

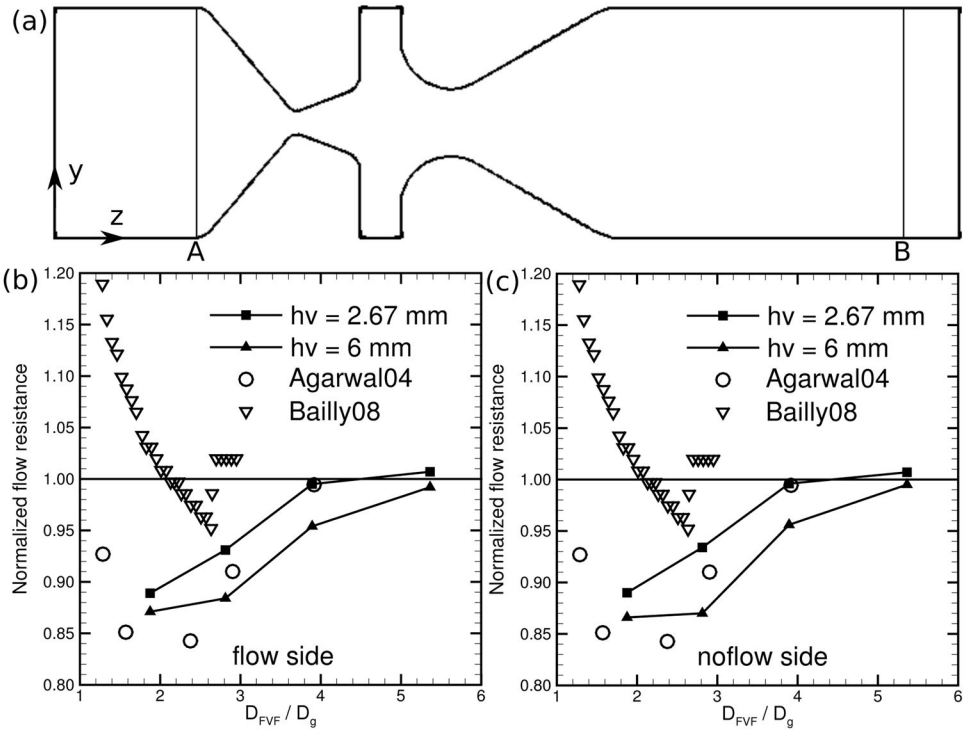

Figure 7.
Normalized flow resistance with respect to the baseline case between planes A and B.

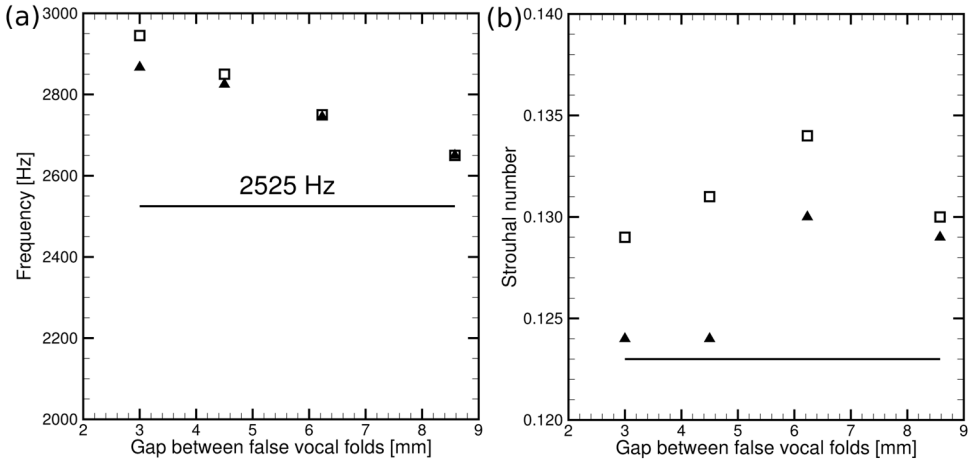

Figure 8.

(a) Frequency of the highest spectral peak vs the gap between the FVFs and (b) Strouhal number vs the gap between the FVFs. The square represents h_v = 2.67 mm and the black triangle h_v = 6 mm.

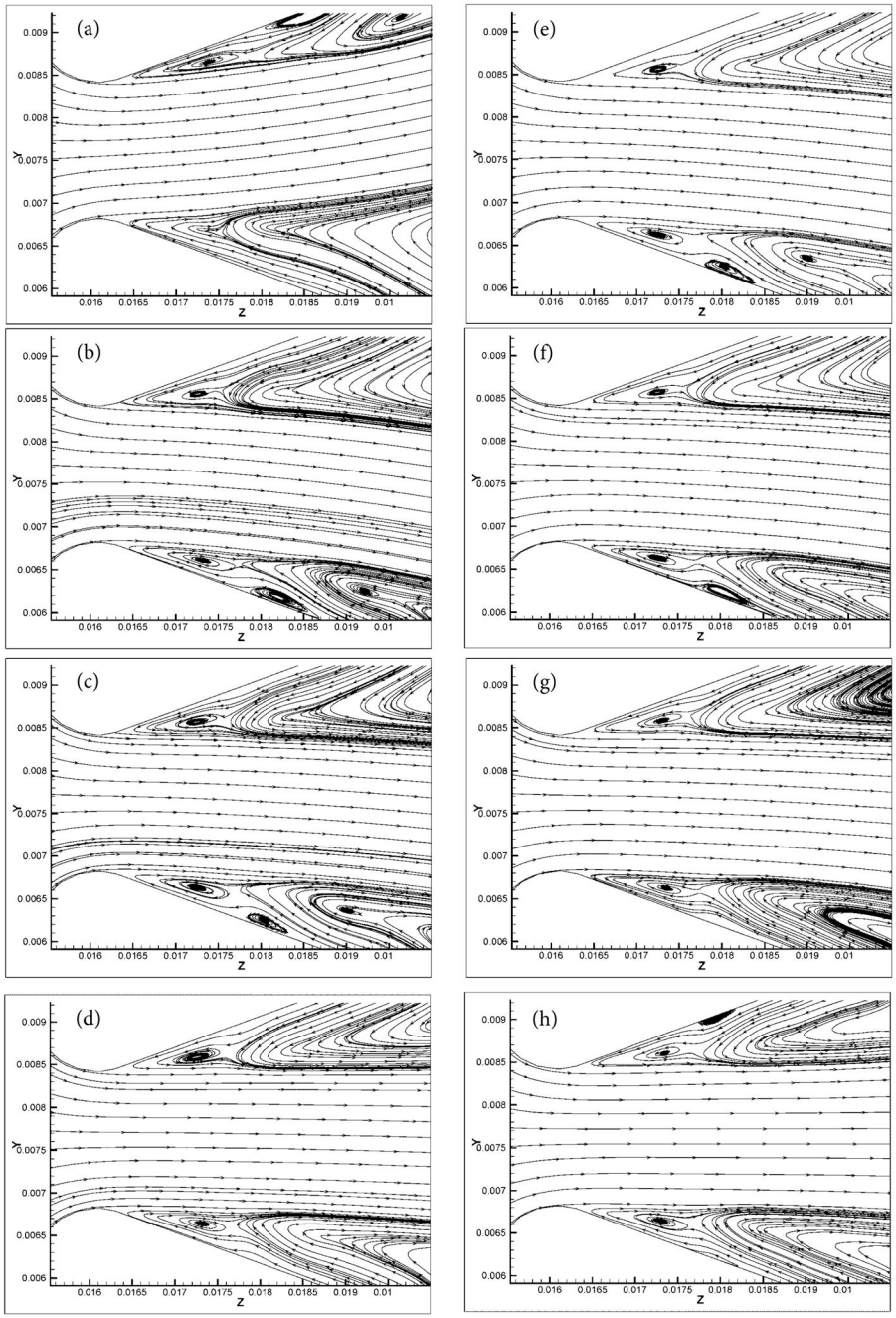

Figure 9.

Streamlines of in-plane velocity for h_v = 2.67 mm (a,b,c,d) and h_v = 6 mm (e,f,g,h), in the diverging region of the TVFs

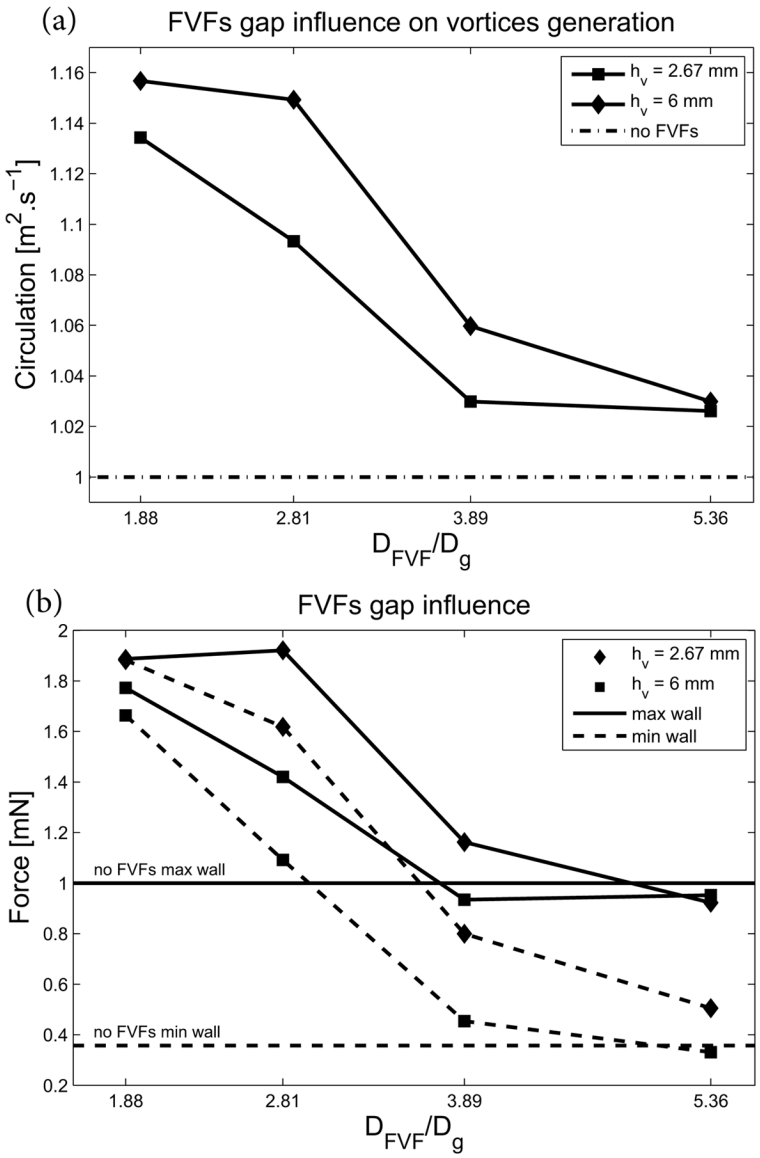

Figure 10.

(a) Normalized circulation in the diverging region of the TVFs. (b) Normalized forces applied on the diverging walls of the TVFs